Recurrent *MET* fusion genes represent a druggable target in paediatric glioblastoma

Sebastian Bender[1,2,3,*], Jan Gronych[3,4,*], Hans-Jörg Warnatz[5,*], Barbara Hutter[6,*], Susanne Gröbner[1,3], Marina Ryzhova[7], Elke Pfaff[1,2,3], Volker Hovestadt[3,4], Florian Weinberg[8,9], Sebastian Halbach[8], Marcel Kool[1,3], Paul A. Northcott[1,3], Dominik Sturm[1,3], Lynn Bjerke[10], Thomas Zichner[11], Adrian M. Stütz[11], Kathrin Schramm[3,4], Bingding Huang[12], Ivo Buchhalter[6,12], Michael Heinold[6], Thomas Risch[5], Barbara C. Worst[1,2,3], Cornelis M. van Tilburg[2,3,13], Ursula D. Weber[3,4], Marc Zapatka[3,4], Benjamin Raeder[11], David Milford[14], Sabine Heiland[14], Christof von Kalle[15], Christopher Previti[16], Chris Lawerenz[12], Andreas E. Kulozik[2], Andreas Unterberg[17], Olaf Witt[2,18], Andreas von Deimling[3,19,20], David Capper[3,19,20], Nathalène Truffaux[21], Jacques Grill[21], Nada Jabado[22], Astrid M. Sehested[23], David Sumerauer[24], Dorra Hmida-Ben Brahim[25], Saoussen Trabelsi[25], Ho-Keung Ng[26], David Zagzag[27], Jeffrey C. Allen[28], Matthias A. Karajannis[28], Nicholas G. Gottardo[29,30,31], Chris Jones[10], Jan O. Korbel[11], Sabine Schmidt[16], Stephan Wolf[16], Guido Reifenberger[32], Jörg Felsberg[32], Benedikt Brors[3,6,13], Christel Herold-Mende[17], Hans Lehrach[5], Tilman Brummer[8,9,33,34] Andrey Korshunov[3,19,20], Roland Eils[12,35,36], Marie-Laure Yaspo[5], Stefan M. Pfister[1,2,3,#,@], Peter Lichter[3,4,#,@], and David T.W. Jones[1,3,#,@] for the International Cancer Genome Consortium PedBrain Tumor Project[37]

*These authors contributed equally.

[#]Joint senior authors

@ To whom correspondence should be addressed:

s.pfister@dkfz.de, david.jones@dkfz.de and/or peter.lichter@dkfz.de

Affiliations:

[1]Division of Pediatric Neurooncology, German Cancer Research Center (DKFZ), Heidelberg, Germany

[2]Department of Pediatric Oncology, Hematology & Immunology, Heidelberg University Hospital, Heidelberg, Germany

[3]German Cancer Consortium (DKTK), German Cancer Research Center (DKFZ), Heidelberg, Germany

[4]Division of Molecular Genetics, German Cancer Research Center (DKFZ), Heidelberg, Germany

[5]Max Planck Institute for Molecular Genetics, Berlin, Germany

[6]Division of Applied Bioinformatics, German Cancer Research Center (DKFZ), Heidelberg, Germany

[7]Department of Neuropathology, NN Burdenko Neurosurgical Institute, Moscow, Russia

[8]Institute of Molecular Medicine and Cell Research (IMMZ), Faculty of Medicine, University of Freiburg, Germany

[9]Centre for Biological Signalling Studies *BIOSS*, University of Freiburg, Germany

[10]Divisions of Molecular Pathology and Cancer Therapeutics, The Institute of Cancer Research, Sutton, United Kingdom

[11]European Molecular Biology Laboratory (EMBL), Genome Biology Unit, Heidelberg, Germany

[12]Division of Theoretical Bioinformatics, German Cancer Research Center (DKFZ), Heidelberg, Germany

[13]National Center for Tumor Diseases (NCT), Heidelberg, Germany

[14]Department of Neuroradiology, Heidelberg University Hospital, Heidelberg, Germany

[15]Division of Translational Oncology, German Cancer Research Center (DKFZ) and National Center for Tumor Diseases (NCT), Heidelberg, Germany

[16]Genomics and Proteomics Core Facility, German Cancer Research Center (DKFZ), Heidelberg, Germany

[17]Department of Neurosurgery, Heidelberg University Hospital, Heidelberg, Germany

[18]Clinical Cooperation Unit Pediatric Oncology, German Cancer Research Center (DKFZ), Heidelberg, Germany

[19]Department of Neuropathology, University of Heidelberg, Heidelberg, Germany

[20]Clinical Cooperation Unit Neuropathology, German Cancer Research Center (DKFZ), Heidelberg, Germany

[21]Unité Mixte de Recherche du Centre National de la Recherche Scientifique (CNRS) 8203, Laboratoire de Vectorologie et Thérapeutiques Anticancéreuses and Department of Pediatric and Adolescent Oncology, Institut Gustave Roussy, Université Paris Sud, Villejuif, France

[22]Departments of Pediatrics and Human Genetics, McGill University and the McGill University Health Center Research Institute, Montreal, Canada

[23]Department of Pediatric Hematology and Oncology, Rigshospitalet, Copenhagen, Denmark

[24]Department of Pediatric Hematology and Oncology, 2nd Faculty of Medicine, Charles University and University Hospital Motol, Prague, Czech Republic

[25]Department of Cytogenetics and Reproductive Biology, Farhat Hached Hospital, Sousse, Tunisia

[26]Department of Anatomical and Cellular Pathology, The Chinese University of Hong Kong, Hong Kong, China

[27]Departments of Pathology and Neurosurgery, New York University School of Medicine, New York, USA

[28]Department of Pediatrics, New York University Langone Medical Center, New York, USA

[29]Department of Pediatric Oncology and Haematology, Princess Margaret Hospital for Children, GPO Box D184, Perth, Australia

[30]Telethon Kids Institute, University of Western Australia, PO Box 855, Perth, Australia

[31]School of Pediatrics and Child Health, University of Western Australia, GPO Box D184, Perth, Australia

[32]Department of Neuropathology, Heinrich-Heine-University Düsseldorf, Düsseldorf, Germany

[33]Comprehensive Cancer Center Freiburg CCCF, Medical Center – University of Freiburg, Germany

[34]Deutsches Konsortium für Translationale Krebsforschung (DKTK), Standort Freiburg, Germany

[35]Institute for Pharmacy and Molecular Biotechnology (IPMB), University of Heidelberg, Heidelberg, Germany

[36]BioQuant Center, University of Heidelberg, Heidelberg, Germany

[37]http://www.pedbraintumor.org

Abstract

Paediatric glioblastoma is one of the most common and most deadly brain tumours in childhood. Here we describe an integrative genetic analysis of 53 paediatric glioblastomas and 5 *in vitro* model systems, leading to the identification of previously unidentified gene fusions involving the MET oncogene in ~10% of cases. These MET fusions activate mitogen-activated protein kinase (MAPK) signalling and, in cooperation with lesions compromising cell cycle regulation, induce aggressive glial tumours *in vivo*. MET inhibitors suppressed MET tumour growth in xenograft models. Finally, we treated a paediatric patient bearing a MET fusion-expressing GBM with the targeted inhibitor crizotinib. This therapy led to substantial tumour shrinkage and associated relief of symptoms but simultaneous appearance of new treatment-resistant lesions, indicating that combination therapies are likely needed to achieve a durable clinical response.

Paediatric glioblastoma is a deadly childhood tumour characterised by a complex genomic landscape and profound heterogeneity[1-3]. Certain canonical pathways, however, such as the mitogen-activated protein kinase (MAPK) or phosphatidylinositol 3-kinase (PI3K) pathways, are frequently deregulated. The identification of recurrent mutations of histone H3-encoding genes (most commonly *H3F3A*) and chromatin modifiers such as *ATRX* also suggests a prominent role for epigenetic deregulation in paediatric glioblastoma[4,5]. Standard treatment is based on unselective radio- and chemotherapy, with marginal clinical benefit. No molecularly-targeted therapy is used as yet. Patient outcomes remain dismal, and novel targets for individualised or molecularly-stratified therapies are desperately needed.

We performed whole-genome sequencing of tumour and blood DNA of 53 samples, as well as five paediatric glioblastoma cell lines covering the whole spectrum of recurrent H3.3 mutations, in the context of the International Cancer Genome Consortium (ICGC) PedBrain Tumour project (Fig. 1 and Supplementary Table 2, 3). Genome-wide DNA methylation analysis on our cohort showed that, in addition to the previously described epigenetic subgroups[6], five of the tumours molecularly resembled pleomorphic xanthoastrocytoma (PXA)[7] - a less aggressive brain tumour with heterogeneous appearance[3] (Supplementary Fig. 1). The full tumour cohort is described in Supplementary Tables 1 & 2. Two of five PXA-like tumours carried lesions typical of PXAs (*BRAF* V600E and deletion of *CDKN2A/B*)[8,9]. Moreover, one potential PXA (ICGC_GBM34) in an infant was found to harbour a gene fusion between *Ets variant 6* (*ETV6*) and the *neurotrophin receptor type 2* (*NTRK2*) gene. This fusion, and others involving *NTRK*-family genes, were recently described in 40% of infant glioblastomas[10] and some lower-grade gliomas[11,12]. Analogous to the highly oncogenic FGFR1–TACC1 and FGFR3–TACC3 fusions in

glioblastoma[13], we found a novel fusion of *fibroblast growth factor receptor 2* (*FGFR2*) with *CAP-GLY domain containing linker protein 2* (*CLIP2*) in a molecular PXA primary-relapse pair (ICGC_GBM19&50) (Supplementary Table 4).

Three paediatric glioblastomas whose DNA methylation profiles clustered together with normal brain samples (suggesting high normal cell content) showed notably lower-than-expected mutant allele frequencies (Supplementary Fig. 2).

A full overview of genetic alterations is provided in Figure 1 and Supplementary Table 3. The most commonly altered pathway was cell cycle regulation, with mutations in *TP53* or *PPM1D*, or homozygous deletion of *CDKN2A/B*, identified in 83% of all samples. We also detected numerous genetic lesions likely to result in aberrantly activated receptor tyrosine kinase (RTK)-PI3K-MAPK signalling, including activating mutations of RTKs (e.g. *EGFR*) or downstream proteins (e.g. *NRAS*, *KRAS*, *BRAF* and *PIK3CA*) and high-level gene amplifications of *EGFR*, *PDGFR/KIT* or *MET* (Fig. 1). ICGC_GBM17 harboured a novel splice site mutation within intron 12 of *NTRK3*, likely resulting in an amino-terminally truncated protein maintaining the catalytically active NTRK3 kinase domain (Supplementary Fig. 3). Other common features included a high frequency of dramatic structural rearrangements (chromothripsis)[14], hypermutated tumours (prior to any adjuvant therapy, and often associated with germline mismatch repair deficiency[15]) and alterations in telomere maintenance. Analysis of five primary-recurrent tumour pairs indicated that known somatic driver events were typically shared between both lesions, with the exception of ICGC_GBM11 & ICGC_GBM71 (which were clinically reported as two anatomically distinct lesions) (Supplementary Fig. 4). Interestingly, different *BCOR* gene mutations were detected in the primary tumour (ICGC_GBM4, *BCOR* F206fs) and

both recurrent tumours (ICGC_GBM36, *BCOR wildtype* and ICGC_GBM49, *BCOR* V1112fs) of one patient (Supplementary Fig. 4).

RNA sequencing revealed fusion transcripts resulting from structural rearrangements in most samples (27/42, 64%; Supplementary Table 4). These often involved known cancer-associated genes such as *FGFR2, NTRK2*, and *PIK3R2*. The most frequently affected gene was the oncogenic tyrosine kinase *MET*. We detected two novel fusions of MET, retaining only the carboxy-terminal kinase domain. In ICGC_GBM1, the MET kinase domain was fused to *TRK-fused gene* (*TFG*), previously described to form chimeric proteins with other RTKs such as *NTRK1* in papillary thyroid carcinoma or *ALK* in anaplastic large-cell lymphoma[16,17]. The paediatric glioblastoma cell line SJ-G2 (ICGC_GBM41) harboured a *CLIP2–MET* fusion (Fig. 2a). For the first time in the paediatric setting, we also identified two primary paediatric glioblastomas with a *PTPRZ1–MET* fusion[18]. In this variant, expression of full-length MET is driven from the highly active *PTPRZ1* promoter, leading to MET overexpression (Supplementary Fig. 5a, b). In two additional tumours without RNA-seq data, copy number analysis suggested the presence of a *PTPRZ1–MET* fusion, subsequently confirmed by PCR (ICGC_GBM43 and 71). Dual-colour fluorescence in-situ hybridization (FISH) detected the *PTPRZ1–MET* fusion in tumour sections of ICGC_GBM11, 15 and 71 (Supplementary Fig. 5c). ICGC_GBM43 (H3.3 G34R) was the only histone H3.3-mutant tumour harbouring a *MET* fusion and amplification. Notably, all paediatric glioblastomas bearing a *MET* fusion were found to have impaired cell cycle regulation due to *TP53* mutation or homozygous deletion of the *CDKN2A/B* locus (Fig. 1). MET fusion-bearing paediatric glioblastomas did not cluster as a group using DNA methylation or gene expression data. None of the tumours expressed the short variant of *MET* lacking exons 7 and 8, which was recently described in 6% of high-grade gliomas[19].

Overexpression of HA-tagged TFG–MET or PTPRZ1–MET in HEK293T cells resulted in phosphorylation of tyrosines Y1234/1235 within the activation loop of the kinase domain (Fig. 2b). Moreover, this overexpression induced strong activation of MAPK signalling as indicated by substantially elevated pERK levels (Fig. 2B), and resulted in cell rounding and detachment (Supplementary Fig. 6a)[20]. Interestingly, the amino-terminally truncated fusions showed much higher downstream activity than the full-length, *PTPRZ1*-driven variant (Fig. 2b).

To further characterise induced transcriptional changes in a model which better mimics the presumed origins of paediatric glioblastoma, we generated expression profiles of TFG–MET-overexpressing normal human astrocytes (NHAs). Transduced cells displayed a phenotypic change indicative of transformation (Supplementary Fig. 6a,b), together with altered expression of multiple factors involved in MAPK signalling (e.g. MAP2K3, MAP2K6, DUSP14) as well as downstream transcription factors (e.g. FOS, JUN) (Supplementary Fig. 6c and Supplementary Table 5).

TFG–MET-overexpressing cells were subsequently treated with the MET inhibitors foretinib, SGX523 or crizotinib, which abrogated MET fusion-induced MAPK activation (Fig. 2b, c). In CLIP2–MET-expressing SJ-G2 cells, foretinib reduced cell viability in a concentration-dependent manner, resulting in an IC_{50} of 0.8µM. In three paediatric glioblastoma cell lines without MET fusion, the IC50 was substantially higher (2-13.5µM; Supplementary Fig. 6d). Although the methylated *MGMT* promoter may suggest sensitivity to alkylating therapy, temozolomide (the current standard chemotherapeutic for paediatric glioblastoma) did not affect the viability of SJ-G2 cells even at concentrations >300µM (Supplementary Fig. 6e). Anchorage-independent growth of these cells was also completely abolished in the presence of 0.5µM foretinib (Supplementary Fig. 6f).

To test the oncogenicity of MET fusions *in vivo*, we used the RCAS/Tv-a somatic gene transfer system to introduce the TFG–MET fusion (PTPRZ1–MET fusions exceed the RCAS insert size limit of ~2.5 kb) into nestin-positive cells of wild-type (Ntv-a), Cdkn2a-deficient (Ntv-a;Cdkn2a$^{-/-}$;Pten$^{fl;fl}$) or p53-null (Ntv-a;Trp53$^{-/-}$) neonatal mice. While no tumours could be found in wild-type mice (n=7) by 12 weeks after injection, Cdkn2a$^{-/-}$ (n=7) and Trp53$^{-/-}$ mice (n=5) rapidly developed severe neurological symptoms and extensive contrast-enhancing lesions (Fig. 3a, b). Neuropathological evaluation indicated histology characteristic for high-grade glioma, and immunohistochemistry detected expression of the HA-tagged fusion protein as well as phosphorylated MET and Erk (Fig. 3c). A contribution of off-target viral mutagenesis to tumourigenesis in this system can be excluded based on previously published data[21] and our own unpublished observations (J. Gronych).

Due to the rapid growth of RCAS-driven tumours and the lack of reliable techniques for oral drug delivery in infant mice (<p10), we used luciferase-labelled RCAS-TFG–MET-driven mouse tumour cells allografted into the striatum of 6-8 week old immunocompromised mice to assess pharmacological MET inhibition *in vivo*. One week after transplantation, animals were split into two groups with similar distributions of luminescence intensity and subsequently subjected to a 60mg/kg foretinib vs. vehicle one day on/one day off treatment regimen. Foretinib treatment significantly decelerated MET fusion-driven tumour growth (Supplementary Fig. 6g) leading to prolonged overall survival (Fig. 3d).

To confirm our results, we established a xenograft model using luciferase-labelled SJ-G2 cells endogenously harbouring the *CLIP2–MET* fusion transplanted intracranially into NSG mice. Tumour growth was monitored once a week by intravital bioluminescence imaging (Fig. 3e). While all of the vehicle-treated animals showed a clear increase in luminescence signal, the

signal in foretinib-treated animals stagnated or even decreased under treatment. All foretinib-treated animals were still alive at the end of the two week treatment, while 6/7 of the untreated animals had died (median survival 17 days vehicle vs. 26 days foretinib, p=0.0001; Fig. 3f). Western blot analysis showed reduced ERK phosphorylation in tumour tissue of the foretinib-treated animals, indicating successful target inhibition and reduced downstream signalling (Fig. 3g).

Finally, we were able to translate these findings into clinical application within the pilot phase of the INFORM personalised oncology program[22] (German Clinical Trials Register ID: DRKS00007623). Whole-exome, low-coverage whole-genome (for copy number annotation) and RNA sequencing was performed on a recurrent lesion from an 8-year old male patient treated three years previously for a group 3 medulloblastoma (INF_51_XT1). This revealed the presence of a *PTPRZ1–MET* fusion in the recurrent tumour, and subsequent molecular and histological review indicated that this lesion was in fact a cerebellar glioblastoma (i.e. most likely a radiation-induced secondary glioblastoma) (Fig. 4a). On this basis, the patient received treatment with crizotinib (an FDA-approved kinase inhibitor with activity against MET), which was previously shown to induce tumour regression of a MET-amplified glioblastoma[23]. MRI evaluation two months after treatment initiation revealed a partial response of the primary lesion with concomitant relief of symptoms. However, several new treatment resistant lesions were also observed. Rapid progression of those lesions ultimately resulted in death of the patient (Fig. 4b). No autopsy material was available for studying the resistance mechanism.

Oncogenic activation of MET signalling is found in numerous human malignancies, including cancer of the hematopoietic system, carcinomas, sarcomas as well as glioblastomas[24,25]. In paediatric glioblastomas, *MET* gene amplification has been described in about 3-7% of

tumours[10,26], while our data suggest MET fusions in up to 10% of cases. Interestingly, the structural alterations in ICGC_GBM11 & 71, representing two lesions from one patient, suggest that distinct *PTPRZ1–MET* fusions arose separately in each tumour. High clonality of the *PTPRZ1–MET* fusion, as indicated by our FISH data, further underlines the likely tumour-initiating character of this fusion, which seems to rely on extremely high expression of full-length MET driven by the *PTPRZ1* promoter. The amino-terminally truncated versions, however, represent cytosolic, constitutively active forms of MET, which escape normal down-regulation[27]. The latter are analogous to the oncogenic *TPR–MET* fusion originally identified in mutagen-treated osteosarcoma cells[28]. A recent screen of TCGA data from multiple tumour types (http://www.tumourfusions.org)[29] revealed a small number of *MET* fusions, including one *TFG–MET* fusion, in breast, lung and thyroid cancer, suggesting that *MET* rearrangements may have a broader role across tumour entities.

Our data suggest that MET fusion-induced tumourigenesis is dependent on additional genetic lesions affecting cell cycle regulation. All seven paediatric glioblastomas bearing a MET fusion harboured mutations of *TP53* or deletions of *CDKN2A/B*. Accordingly, overexpression of TFG–MET in neural progenitor cells induced aggressive glial brain tumours in Cdkn2a- or Trp53-deficient mice, but not in wildtype animals.

On the basis of our preclinical allograft and xenograft data, pharmacological MET inhibition was immediately translated into clinical application by treating a child with a *PTPRZ1–MET* fusion-driven paediatric glioblastoma with a MET inhibitor, leading to relief of symptoms over a period of two months and substantial volume reduction of the primary tumour. Unfortunately, novel lesions that developed rapidly under crizotinib monotherapy ultimately lead to a fatal outcome. Since acquired resistance to MET inhibition is a well-known challenge in the treatment of

numerous cancers[30,31], combinatorial inhibition of multiple RTKs, as recently described in diffuse intrinsic pontine gliomas (DIPGs)[32], might represent a promising therapeutic option.

In conclusion, our results highlight a new recurrent mechanism of tumourigenesis in paediatric glioblastoma, and underline the importance of individualised molecular diagnosis for cancer patients as a basis for optimal personalised therapy. Our data also provides strong rationale for the systematic analysis of MET inhibitors in future paediatric glioblastoma clinical trials.

Accession codes

Short-read sequencing and methylation data are available at the European Genome-phenome Archive (EGA, http://www.ebi.ac.uk/ega/) hosted by the EBI under the accession number EGAS00001001139.

Acknowledgements

For technical support and expertise we thank A. Wittmann, L. Sieber, C. Xanthopoulos, D. Sohn and N. Mack, the DKFZ Genomics and Proteomics Core Facility, the DKFZ Center for Preclinical Research, R. Kabbe (Division of Theoretical Bioinformatics, DKFZ), M. Bieg and M. Schlesner (Division of Applied Bioinformatics, DKFZ), C. Jäger-Schmidt (Data Management Group, DKFZ), S. Rüffer and T. Giese from the Heidelberg University Hospital, M. Rabenstein from the NCT Heidelberg, S. Thamm, D. Balzereit, S. Dökel, M. Linser, A. Kovacsovics and V. Amstislavskiy from the Max Planck Institute for Molecular Genetics (MPIMG) in Berlin, the tissue bank of the National Center for Tumor Diseases (NCT, Heidelberg) and the Department of Oncogenomics (University of Amsterdam). Ntv-a;Cdkn2a$^{-/-}$;Pten$^{fl;fl}$ mice were kindly provided by E. Holland (Fred Hutchinson Cancer Research Center).

This work was principally supported by the PedBrain Tumour Project contributing to the International Cancer Genome Consortium, funded by German Cancer Aid (109252) and by the German Federal Ministry of Education and Research (BMBF, grants #01KU1201A, MedSys #0315416C, NGFNplus #01GS0883 and e:Med Joint Research Projects SYS-GLIO #031A425A and CancerTelSys #01ZX1302). Additional support came from the German Cancer Research

Center – Heidelberg Center for Personalized Oncology (DKFZ-HIPO), the German Cancer Consortium (DKTK, INFORM project), the Max Planck Society (Munich, Germany), the European Union (FP7/2007-2013, grant ESGI #262055), the Helmholtz Alliance Preclinical Comprehensive Cancer Center (PCCC, grant number HA-305), the German Research Foundation (DFG, grant LA2983/2-1), the EDM and the Lemos Foundations, the New York University Langone Human Specimen Resource Center, Laura and Isaac Perlmutter Cancer Center, supported in part by the Cancer Center Support Grant, P30 CA16087 from the National Cancer Institute, National Institutes of Health, UL 1 TR000038 from the National Center for the Advancement of Translational Science (NCATS), National Institutes of Health, and grants from the Making Headway Foundation. J. Gronych was supported by a Dr. Mildred Scheel Foundation Scholarship. The authors acknowledge NHS funding to the NIHR Biomedical Research Centre at The Royal Marsden and the ICR as well as the project (Ministry of Health, Czech Republic) for conceptual development of research organization 00064203 (University Hospital Motol, Prague, Czech Republic).

Author Contributions

S.B., J.G., H-J.W., E.P., F.W., S.H., D.S., L.B., A.M.S., K.S., B.R., D.M., S.He., C.v.K., S.Sch., S.W., J.F., T.B. performed and/or coordinated experimental work.

S.B., J.G., H-J.W., B.H., S.G., V.H., M.K., P.A.N., T.Z., B.Hua, M.R., I.B., M.H., T.R., M.Z., C.P., C.L., B.W. performed data analysis.

M.R., A.E.K., A.U., O.W., A.v.D., D.C., N.J., A.M.Se., D.Su., M.A.K., C.J., C.H-M., A.K., J.Gr, N.T., C.M.v.T., B.W., D.H-B.B., S.T., H-K.N., D.Z., J.C.A., N.G. collected data and provided patient materials.

S.B., J.G., H-J.W., B.H., S.M.P., P.L. and D.T.W.J. prepared the initial manuscript and figures.

S.B., J.G., U.D.W., J.O.K., G.R., B.B., H.L., T.B., R.E., M-L.Y., S.M.P., P.L. and D.T.W.J. provided project leadership.

Competing Financial Interests

The authors declare no competing financial interests

References

1 Sturm, D. *et al.* Paediatric and adult glioblastoma: multiform (epi)genomic culprits emerge. *Nature reviews. Cancer* **14**, 92-107, doi:10.1038/nrc3655 (2014).

2 Jones, C. & Baker, S. J. Unique genetic and epigenetic mechanisms driving paediatric diffuse high-grade glioma. *Nature reviews. Cancer* **14**, doi:10.1038/nrc3811 (2014).

3 Louis, D. N. *et al. WHO Classification of Tumours of the Central Nervous System, Revised. Fourth Edition*. (IARC, 2016).

4 Wu, G. *et al.* Somatic histone H3 alterations in pediatric diffuse intrinsic pontine gliomas and non-brainstem glioblastomas. *Nature genetics* **44**, 251-253, doi:10.1038/ng.1102 (2012).

5 Schwartzentruber, J. *et al.* Driver mutations in histone H3.3 and chromatin remodelling genes in paediatric glioblastoma. *Nature* **482**, 226-231, doi:10.1038/nature10833 (2012).

6 Sturm, D. *et al.* Hotspot mutations in H3F3A and IDH1 define distinct epigenetic and biological subgroups of glioblastoma. *Cancer cell* **22**, 425-437, doi:10.1016/j.ccr.2012.08.024 (2012).

7 Korshunov et al. Integrated analysis of pediatric glioblastoma reveals a subset of biologically favorable tumors with associated molecular prognostic markers. *submitted*.

8 Dias-Santagata, D. *et al.* BRAF V600E mutations are common in pleomorphic xanthoastrocytoma: diagnostic and therapeutic implications. *PloS one* **6**, e17948, doi:10.1371/journal.pone.0017948 (2011).

9 Weber, R. G. *et al.* Frequent loss of chromosome 9, homozygous CDKN2A/p14(ARF)/CDKN2B deletion and low TSC1 mRNA expression in pleomorphic xanthoastrocytomas. *Oncogene* **26**, 1088-1097, doi:10.1038/sj.onc.1209851 (2007).

10 Wu, G. *et al.* The genomic landscape of diffuse intrinsic pontine glioma and pediatric non-brainstem high-grade glioma. *Nature genetics* **46**, 444-450, doi:10.1038/ng.2938 (2014).

11 Jones, D. T. *et al.* Recurrent somatic alterations of FGFR1 and NTRK2 in pilocytic astrocytoma. *Nature genetics* **45**, 927-932, doi:10.1038/ng.2682 (2013).

12 Zhang, J. *et al.* Whole-genome sequencing identifies genetic alterations in pediatric low-grade gliomas. *Nature genetics* **45**, 602-612, doi:10.1038/ng.2611 (2013).

13 Singh, D. *et al.* Transforming fusions of FGFR and TACC genes in human glioblastoma. *Science* **337**, 1231-1235, doi:10.1126/science.1220834 (2012).

14 Stephens, P. J. *et al.* Massive genomic rearrangement acquired in a single catastrophic event during cancer development. *Cell* **144**, 27-40, doi:10.1016/j.cell.2010.11.055 (2011).

15 Shlien, A. *et al.* Combined hereditary and somatic mutations of replication error repair genes result in rapid onset of ultra-hypermutated cancers. *Nature genetics* **47**, 257-262, doi:10.1038/ng.3202 (2015).

16 Greco, A. *et al.* The DNA rearrangement that generates the TRK-T3 oncogene involves a novel gene on chromosome 3 whose product has a potential coiled-coil domain. *Molecular and cellular biology* **15**, 6118-6127 (1995).

17 Hernandez, L. *et al.* TRK-fused gene (TFG) is a new partner of ALK in anaplastic large cell lymphoma producing two structurally different TFG-ALK translocations. *Blood* **94**, 3265-3268 (1999).

18 Bao, Z. S. *et al.* RNA-seq of 272 gliomas revealed a novel, recurrent PTPRZ1-MET fusion transcript in secondary glioblastomas. *Genome research*, doi:10.1101/gr.165126.113 (2014).

19 Navis, A. C. *et al.* Identification of a novel MET mutation in high-grade glioma resulting in an auto-active intracellular protein. *Acta neuropathologica*, doi:10.1007/s00401-015-1420-5 (2015).

20 Laser-Azogui, A., Diamant-Levi, T., Israeli, S., Roytman, Y. & Tsarfaty, I. Met-induced membrane blebbing leads to amoeboid cell motility and invasion. *Oncogene* **33**, 1788-1798, doi:10.1038/onc.2013.138 (2014).

21 Shin, C. H., Grossmann, A. H., Holmen, S. L. & Robinson, J. P. The BRAF kinase domain promotes the development of gliomas in vivo. *Genes Cancer* **6**, 9-18, doi:10.18632/genesandcancer.48 (2015).
22 Worst, B. C. *et al.* Next-generation personalised medicine for high-risk paediatric cancer patients - The INFORM pilot study. *Eur J Cancer* **65**, 91-101, doi:10.1016/j.ejca.2016.06.009 (2016).
23 Chi, A. S. *et al.* Rapid radiographic and clinical improvement after treatment of a MET-amplified recurrent glioblastoma with a mesenchymal-epithelial transition inhibitor. *Journal of clinical oncology : official journal of the American Society of Clinical Oncology* **30**, e30-33, doi:10.1200/JCO.2011.38.4586 (2012).
24 Birchmeier, C., Birchmeier, W., Gherardi, E. & Vande Woude, G. F. Met, metastasis, motility and more. *Nature reviews. Molecular cell biology* **4**, 915-925, doi:10.1038/nrm1261 (2003).
25 Gherardi, E., Birchmeier, W., Birchmeier, C. & Vande Woude, G. Targeting MET in cancer: rationale and progress. *Nature reviews. Cancer* **12**, 89-103, doi:10.1038/nrc3205 (2012).
26 Brennan, C. W. *et al.* The somatic genomic landscape of glioblastoma. *Cell* **155**, 462-477, doi:10.1016/j.cell.2013.09.034 (2013).
27 Mak, H. H. *et al.* Oncogenic activation of the Met receptor tyrosine kinase fusion protein, Tpr-Met, involves exclusion from the endocytic degradative pathway. *Oncogene* **26**, 7213-7221, doi:10.1038/sj.onc.1210522 (2007).
28 Cooper, C. S. *et al.* Molecular cloning of a new transforming gene from a chemically transformed human cell line. *Nature* **311**, 29-33 (1984).
29 Yoshihara, K. *et al.* The landscape and therapeutic relevance of cancer-associated transcript fusions. *Oncogene*, doi:10.1038/onc.2014.406 (2014).
30 Diamond, J. R. *et al.* Initial clinical sensitivity and acquired resistance to MET inhibition in MET-mutated papillary renal cell carcinoma. *Journal of clinical oncology : official journal of the American Society of Clinical Oncology* **31**, e254-258, doi:10.1200/JCO.2012.46.4289 (2013).
31 Lai, A. Z. *et al.* Dynamic reprogramming of signaling upon met inhibition reveals a mechanism of drug resistance in gastric cancer. *Science signaling* **7**, ra38, doi:10.1126/scisignal.2004839 (2014).
32 Truffaux, N. *et al.* Preclinical evaluation of dasatinib alone and in combination with cabozantinib for the treatment of diffuse intrinsic pontine glioma. *Neuro-oncology*, doi:10.1093/neuonc/nou330 (2014).
33 Mosse, Y. P. *et al.* Safety and activity of crizotinib for paediatric patients with refractory solid tumours or anaplastic large-cell lymphoma: a Children's Oncology Group phase 1 consortium study. *Lancet Oncol* **14**, 472-480, doi:10.1016/S1470-2045(13)70095-0 (2013).

Figure Legends

Figure 1. The genomic landscape of pediatric glioblastomas. Genetic alterations (mutations, small insertions/deletions (InDels), focal copy number alterations and fusions) identified by whole-genome (n=52) or whole-exome/ low-coverage whole-genome (INF_51_XT1) and RNA-sequencing (n=42) in 19 midline and 29 hemispheric pediatric glioblastomas, 5 PXA-like tumours as well as 5 pediatric glioblastoma cell lines. Frequencies of genetic alterations [%] in 58 analysed samples are indicated at the end of each row. Numbers given in row 'Recurrent tumour' indicate ICGC-IDs of primary tumours.

Figure 2. Oncogenic MET fusions. (**a**) Schematics of wild-type MET and fusion proteins identified in pediatric glioblastomas. The MET polypeptide precursor is composed the extracellular domain (ED), the transmembrane domain (TM), juxtamembrane domain (JM), kinase domain (KD), and carboxy-terminal domain (CT). Tyrosine 1003 (Y1003) negatively regulates MET by recruiting ubiquitin ligases. Tyrosines 1234 and 1235 (Y1234/Y1235) are critical for MET activation. TFG–MET and CLIP2–MET maintain only the kinase domain, while PTPRZ1–MET fusion proteins contain full-length MET. (**b**) HA-tagged MET fusions (TFG–MET or PTPRZ1–MET) or wild-type MET were expressed in HEK293 cells. Abundance of indicated proteins was measured by immunoblot. Cells were treated with 0.5µM foretinib for 24h where indicated. Proteins at 140 kDA represent endogenous (wild-type) MET or overexpressed PTPRZ1–MET-HA, overexpressed TFG–MET-HA protein has a molecular weight of 65 kDa. (**c**) MET fusion overexpressing HEK293T cells were treated where indicated with the MET inhibitors foretinib (0.5µM), SGX523 (1µM) or crizotinib (1µM) for 24h. kDa = kilodaltons.

Figure 3. MET fusion animal model and preclinical testing of a MET inhibitor. (**a**) $1x10^5$ DF-1 cells producing RCAS-TFG–MET-HA viral particles where injected into the cerebral

hemisphere of neonatal Ntv-a;Cdkn2a$^{-/-}$;Pten$^{fl;fl}$ animals. MRI imaging (T1 RARE) of an Ntv-a;Cdkn2a$^{-/-}$;Pten$^{fl;fl}$ animal two weeks after inoculation with RCAS-TFG–MET-HA virus. Scale bars = 1mm. (**b**) Kaplan-Meier survival analysis of wild type (Ntv-a), Cdkn2a-null (Ntva;Cdkn2a$^{-/-}$;Pten$^{fl;fl}$) and and p53-null (Ntv-a;Trp53-/-) animals inoculated with RCAS-TFG–MET. (p=0.0001). (**c**) Histologic analysis of a tumour induced by overexpression of TFG–MET in Ntv-a; Cdkn2a$^{-/-}$; Pten$^{fl;fl}$ animals. Scale bars = 100µm. (**d**) Luciferase-labelled murine RCAS-TFG–MET tumour cells where implanted into the striatum of adult CB17 SCID mice and treated with 60 mg/kg foretinib (n=10) or vehicle (n=10), respectively, every other day starting one week after surgery. Kaplan-Meier analysis of survival indicates a significant survival benefit for animals treated with foretinib ($p<0.0001$). (**e**) CB17 SCID animals were transplanted with luciferase-labeled CLIP2–MET-expressing SJ-G2 cells and subjected to intravital bioluminescence imaging once a week. Mice were treated with 60 mg/kg foretinib (n=7) or vehicle (n=7), respectively, every other day starting from day 7 after surgery. Intravital bioluminescence imaging was performed once a week. Scale bars = 5mm. (**f**) Kaplan-Meier analysis of the mice described in panel e ($p<0.0001$). (**g**) Immunoblot analysis of protein extracts from SJ-G2 xenografts of a foretinib treated and an untreated (vehicle) animal from an independent experiment with antibodies detecting phosphorylated ERK (T202/Y204). RAB11 is shown as a loading control.

Figure 4. Translation of MET inhibitor treatment into a clinical setting. (**a**) Immunohistochemical staining for H&E, GFAP and pMET (Y1234/Y1235) of the primary medulloblastoma (upper panels) and the PTPRZ1–MET-expressing pediatric glioblastoma (lower panels) in patient INF_51_XT1. Scale bars = 100µm. (**b**) All images represent axial T1-weighted

MRI-scans with contrast enhancement of patient INF_51_XT1 at baseline and at indicated time points after initiation of treatment. Crizotinib was given at 2x 250mg/d p.o. (equivalent to 2x 280mg/m^2, published recommended phase II dose[33]) for 11 weeks, with a pause from day 13-16. Marked tumour shrinkage corresponding to a partial response at the site of the main lesion (arrows). New lesions also developed during the course of treatment (arrowheads). Scale bars = 5cm.

Online Methods

Patient and Tumour Samples

Informed consent of all patients as well as an ethical vote (Ethics Committee of the Medical Faculty of Heidelberg) was obtained according to ICGC guidelines. Tumour tissues were subjected to neuropathological review to confirm histology and tumour cell content.

DNA sequencing

Paired-end library preparation was conducted using Illumina v2 protocols. Genomic DNA (~1 µg) was fragmented to an insert size of ~300 bp with a Covaris device, and size selection was performed using agarose gel excision. Deep sequencing was carried out with Illumina HiSeq 2000 instruments.

RNA sequencing

RNA integrity was evaluated by using a Bioanalyzer 2100 instrument (Agilent, Palo Alto, CA). Stranded paired-end libraries were prepared from 1 µg RNA using the Ribo-Zero Gold Kit (Epicentre, Madison, WI). One library per lane was sequenced on a HiSeq 2000 instrument with 2 × 51 bp reads. Gene fusion events were detected by RNA-seq read mapping to the human NCBI37/hg19 reference assembly using SOAPfuse[34] and TopHat2-Fusion[35]. High-confidence events were retained after filtering of common artefacts and visual inspection of RNA-seq coverages on fused exons. Fusion transcripts were annotated based on the Ensembl gene annotation (v70). For fusion transcript validation, 50 ng of total RNAs were reverse transcribed and fused transcripts were amplified using the dART 1-Step RT-PCR Kit (EURx #E0803-02) using primers located upstream and downstream of the transcript breakpoints. RT-PCR products were separated and visualized on 2.5% TBE-agarose gel, excised and purified using the

Zymoclean Gel DNA Recovery Kit (Zymo Research). Capillary Sanger sequencing of 30 ng RT-PCR product was performed with 15 pmol primer (Eurofins MWG Operon).

Mapping and analysis

According to the ICGC-TCGA Pan Cancer Whole Genome workflow, reads were mapped to the 1000 genomes phase 2 assembly of the human reference genome GRCh37 (NCBI build 37.1, downloaded from ftp://ftp.1000genomes.ebi.ac.uk/vol1/ftp/technical/reference/phase2_reference_assembly_sequence) using BWA[36] version 0.7.8 mem with option -T 0. The biobambam package[37] was used to sort the output and to mark PCR duplicates during merging of the per-lane BAM files.

High-level copy number gains were identified by read depth plots and custom Perl scripts.

For detection of single nucleotide variants (SNVs) we used our in-house SNV detection pipeline. The pipeline (manuscripts in preparation) is based on SAMtools mpileup and bcftools[36] version 0.1.19 with parameter adjustments to allow calling of somatic variants with low allele frequency as described previously[38] and heuristic filtering as described by Jones *et al.*[11].

Short insertions and deletions (indels) were identified with Platypus version 0.7.4[39] by providing the tumour and control BAM files. To be of high confidence, somatic calls (control genotype 0/0) are required have the Platypus filter flag PASS or pass custom filters allowing for low variant frequency using a similar scoring scheme as for SNVs. In detail, we discard candidates with the badReads flag, with alleleBias or strandBias if the variant allele frequency is less than 10 %, and indels that have more than two of the remaining flags. Additionally, combinations of Platypus non-PASS filter flags, bad quality values, low genotype quality, very low variant counts in the tumour and presence of variant reads in the control were not tolerated.

All mutations are annotated with ANNOVAR[40] version November 2014, with the Gencode version 19 gene model. Additional information is included by overlapping the genomic positions with dbSNP version 141, 1000 genomes phase1 integrated calls 20101123 and COSMIC version 66. Only somatic, high confidence SNVs and indels were considered for further analysis. We then extracted non-silent coding SNVs, SNVs at splice sites, and indels that fall into a coding gene or splice site. For defining potential somatic SNVs in the cell lines, we discard SNVs and indels known from 1000 genomes or with the dbSNP 141 COMMON=1 flag.

RNA-Seq reads were mapped with STAR version 2.3.0e[41] using an index of the 1000 genomes reference sequence with Gencode version 17 transcript annotations. The output was converted to sorted BAM with SAMtools and duplicates were marked with Picard version tools (http://picard.sourceforge.net, version 1.90).

Expression levels were determined per gene and sample as reads per kilobase of exon model per million reads (RPKM). As the gene model, RefSeq was used. For each gene, overlapping annotated exons from all transcript variants were merged into non-redundant exon units with a custom Perl script. Non-duplicate reads with mapping quality above zero were counted for all exon units with coverageBed from the BEDtools package[42]. The read counts were summarized per gene, then divided by the combined length of its exon units (in kilobases) and the total number of reads (in millions) counted in total by coverageBed.

SNVs and indels were annotated with RNA information by generating a pileup of the DNA variant position in the RNA BAM file with SAMtools. The respective genes, as well as genes in high-level copy number gains, were assigned their expression values.

Chromothripsis was scored in accordance with the criteria outlined by Korbel and Campbell[43].

DNA methylation profiling

For genome-wide assessment of DNA methylation ICGC_GBM samples (n=51) were analysed using the Illumina HumanMethylation450 BeadChip according to the manufacturer's instructions at the DKFZ Genomics and Proteomics Core Facility. In addition, 450k DNA methylation data of 64 reference pediatric glioblastomas described by Sturm *et al.*[6], 16 normal brain samples as well as 7 PXAs was included. DNA methylation probes were filtered as previously described[6]. For unsupervised hierarchical clustering we selected the 2,052 most variably methylated probes across the dataset (s.d. > 0.3). Samples were clustered using 1-Pearson correlation coefficient as the distance measure and average linkage (x-axis). Methylation probes were reordered by hierarchical clustering using euclidean distance and average linkage (y-axis).

Gene expression profiling and classification

Differentially expressed genes (t-test: $p<0.01$) were identified by comparing TFG–MET overexpressing and empty vector transduced normal human astrocytes (NHAs). Classification of tumour samples studied on the Affymetrix U133 Plus2.0 expression array was performed as described in Strum *et al.*[6] using the 840 gene TCGA signature[44].

In vitro studies of MET fusion-expressing HEK293T and SJ-G2 cells

HEK293T and human SJ-G2 glioblastoma cells (authors' long-term stocks) were cultured in high glucose Dulbecco's modified Eagle's medium (DMEM) (Life Technologies) supplemented with 10% fetal calf serum (GIBCO) and penicillin/streptomycin (GIBCO) at 37°C and 5% CO_2. Cells were trypsinised upon reaching a confluency of 80%. Foretinib (Selleck Chemicals) and temozolomide (University Hospital Pharmacy Heidelberg) was dissolved in DMSO and stored at

538 -20°C. Three hours before cell harvest, cell culture medium including inhibitors was replaced.
539 Cell lines were checked for genotype and for mycoplasma before initiation of experiments.

540 Coding sequences of wild-type MET, PTPRZ1–MET or TFG–MET were cloned from tumour
541 cDNA into the pcDNA3.1 vector (Life Technologies) introducing a hemagglutinin (HA) tag.
542 HEK293T cells were transfected using TransIT-LT1 transfection reagent (Mirus).

543 To determine the half-maximum inhibition concentration (IC_{50}) of foretinib and temozolomide,
544 pediatric glioblastoma cell lines were seeded in a 96-well format (opaque-walled) and incubated
545 for 24h in DMEM supplemented with 10% fetal calf serum (GIBCO) and penicillin/streptomycin
546 (GIBCO) at 37°C and 5% CO_2. Subsequently, cells were treated with the indicated concentration
547 of foretinib and temozolomide for additional 24h before replacing the drug-containing medium
548 and incubation for another 24h at 37°C and 5% CO_2. Cell viability was determined in triplicates
549 by using the CellTiter-Glo luminescent cell viability assay (Promega) according to the
550 manufacturer's instructions using a Mithras LB 940 Microplate Reader. Quantification of
551 anchorage-independent growth of SG-G2 cells was determined by using the CytoSelect 96-well
552 cell transformation assay (Cell Biolabs) according to the manufacturer's instructions after the
553 indicated time period. Foretinib- or DMSO-containing DMEM medium was replaced every 24h.

554 **Transduction of Normal Human Astrocytes (NHAs)**

555 The bicistronic retroviral vector pMIBerry has been described previously [45]. In order to generate
556 a pMIBerry vector encoding C-terminally haemagglutinin-tagged TFG–MET, this cDNA was
557 amplified from pLVX/TFG–MET-puro using Phusion polymerase (Finnzymes) and the
558 oligonucleotides XhoITFG–METfwd 5'-
559 AATTCTCGAGATGAACGGACAGTTGGATCTAAGTGGGAAGCTAATC-3' and

BamHITFG–METrev 5'-TTAAAGGATCCTCTAGACTAGGCATAGTCAGGCACGTCATAAGGATATG-3' using the standard protcol supplied by the manufacturer. PCR amplicons were gel purified, digested with XhoI and BamHI and subcloned into XhoI/BamHI linearised pMIBerry. Sanger sequencing confirmed the TFG–MET cDNA sequence.

The culture and transfection of Plat-E cells as well as the generation of retroviral supernatants has been described previously[45]. The immortalized astrocytes were derived from primary normal human astrocytes (NHA; Lot Number 5F1118; Lonza, Cologne/Germany) and were grown in designated astrocyte medium (Lonza) as directed by the manufacturer. For immortalization, 2x 10^6 NHA cells were transiently transfected with 2 µg of pQCXIN/ecoR and the "primary neurons" nucleofector kit (Lonza, Cologne, Germany). This procedure allows for transient expression of the ecotropic receptor used by murine retroviruses, which in turn allows for the infection with ecotropic viral particles as described previously [46]. Two days later, nucleofected cells were infected with the Simian Virus 40 large T antigen (TAg) expression vector pQCXIN/TAg [45]. TAg expressing NHAs were positively selected by TAg mediated suppression of naturally occurring senescence. Subsequently, 2x 10^6 cells were transfected with 2 µg of the plasmid pQCXIN/ecoR. Nucleofected NHA/TAgs were selected with 2 mg/ml G418. The resulting NHATAg-ecoR cells were then incubated with a 1:1 dilution of retroviral supernatants from the indicated pMIG or pMIBerry Plat-E transfectants with astrocyte medium. Infected cells were identified by their dsRed2 autofluorescence 48 h post infection and monitored by flow cytometry.

Immunofluorescence

582 Infected NHA/TAg-ecoR cells were plated on chamber slides (Becton Dickinson) and grown
583 until reaching subconfluency (~72hrs). Cells were then fixed with 4% paraformaldehyde solution
584 for 15 min at RT. Subsequently, F-Actin staining (Phalloidin Alexa 488 (Cell Signaling)) and
585 DAPI ProLong® Gold (LifeTechnologies) were applied according to manufacturers' protocols.
586 Stained cells were imaged with the ZEISS Axio-observer Z1 bright field microscope plus
587 ApoTome 2 with a connected AxioCamMRm. Images were taken with a 40x PlanNeoFluar 1.3
588 oil objective using the AxioVision Rel 4.8 software.

589 **Western Blotting**

590 Protein extract of cell pellets were generated by using RIPA buffer (Sigma) including the Halt
591 Phosphatase Inhibitor Cocktail (Thermo Scientific). Electrophoretic separation of protein samples
592 was performed using 4-12% gradient NuPAGE Bis-Tris Precast Gels (Life Technologies)
593 followed by protein transfer to a polyvinylidene fluoride (PVDF) membrane using a full wet
594 blotting procedure. Antibodies against the following antigens were applied: HA-tag (3724; Cell
595 Signaling; 1:1,000), MET (8198; Cell Signaling; 1:1,000), pMET (3077; Cell Signaling;
596 1:1,000), pERK1/2 (4370; Cell Signaling; 1:2,000) RAB11 (5589; Cell Signaling; 1:2,000) and
597 GAPDH (CB1001; Calbiochem; 1:10,000). Validation of all antibodies is provided on the
598 manufacturer's website.

599 **Fluorescence *in-situ* hybridization (FISH)**

600 Dual-colour interphase FISH was performed on FFPE-embedded tissue sections using a PTPRZ1
601 (RP11-207K20; green) and MET (RP11-95I20; red) specific probe. For each tumour 200
602 interphase nuclei were analysed microscopically.

603 **Animal studies**

All animal experiments were conducted in accordance with legal regulations and approved by the regional council (Regierungspräsidium Tübingen; G-4/11, G-238/12, G-163/14). Mice were housed in IVC caging within the Center for Preclinical Research of the DKFZ and monitored daily for the presence of tumour-related symptoms. Sample sizes were chosen based on minimising the number of animals required to get significant results.

RCAS-based tumour model

For tumour induction using RCAS-based somatic gene transfer the HA-tagged TFG–MET fusion was PCR amplified and cloned into the RCASBP(A) backbone using ClaI and NotI restriction sites. Virus production was done in DF-1 chicken fibroblasts by transfection using FuGene HD (Promega) according to manufacturer´s protocol. Ntv-a, Ntv-a;Cdkn2a$^{-/-}$;Pten$^{fl/fl}$, Ntv-a; Trp53$^{-/-}$ or or Ntv-a;Trp53$^{-/-}$ pups were injected at p0 with 100,000 virus producing cells into the left cerebral hemisphere using a Hamilton syringe.

Xenograft and preclinical studies

Cells derived from Ntv-a;Cdkn2a$^{-/-}$;Pten$^{fl/fl}$ animals injected with RCAS-TFG–MET virus or SJ-G2 tumour cells were labelled with luciferase using pGF lentivirus and subsequently GFP-positive cells were FACS sorted. 500,000 SJ-G2 cells or 100,000 TFG–MET-RCAS cells were transplanted into the striatum of 6-8 weeks old female CB17 SCID (coordinates 2.5mm lat., 1mm caud., 3mm ventr. relative to bregma; animals obtained from Charles River or Janvier Labs, respectively). Animals received pre-emptive Carprofen analgesia and were anaesthetised with Isoflurane. Post-surgically analgesia was continued with Carprofen. For luciferase imaging animals were injected with 100µl Luciferin solution (15mg/ml, Promega) and imaged using an IVIS100 or IVIS Lumia luminescence imager with an exposure time of 5 minutes. For the

treatment studies Foretinib was dissolved in DMSO and then diluted in 5mg/ml hydroxypropyl methylcellulose/0.05% SDS. Animals were randomized to treatment or control strata according to their luminescence signals. 60 mg/kg Foretinib or vehicle was administered non-blinded by oral gavage every other day starting at day 7 after surgery. Kaplan-Meier analysis was done using GraphPad Prism and statistical significance was calculated using a log-rank test.

Magnetic resonance imaging

Magnetic resonance imaging (MRI) was undertaken on a 9.4T horizontal bore NMR scanner (BioSpec 94/20 USR, Bruker BioSpin GmbH, Ettlingen, Germany) with the CryoProbe head coil. A 15 slice T1-weighted RARE (rapid acquisition with relaxation enhancement) sequence, after an i.p. injection of 100µL of a 1:10 dilution of Omniscan (0,5mmol/ml, GE Healthcare Buchler GmbH, Germany), was acquired. The MRI parameters were as follows: TR/TE = 1000/6 ms, matrix = 200 x 150, resolution = 0.1 x 0.1 mm, Slice Thickness/Gap = 0.3/0.3 mm, NA = 2; RARE Factor = 1, Total acquisition time = 5 min.

Methods-only references.

34 Jia, W. *et al.* SOAPfuse: an algorithm for identifying fusion transcripts from paired-end RNA-Seq data. *Genome biology* **14**, R12, doi:10.1186/gb-2013-14-2-r12 (2013).

35 Kim, D. *et al.* TopHat2: accurate alignment of transcriptomes in the presence of insertions, deletions and gene fusions. *Genome biology* **14**, R36, doi:10.1186/gb-2013-14-4-r36 (2013).

36 Li, H. & Durbin, R. Fast and accurate short read alignment with Burrows-Wheeler transform. *Bioinformatics* **25**, 1754-1760, doi:10.1093/bioinformatics/btp324 (2009).

37 Tischler, G., Leonard, S. . biobambam: tools for read pair collation based algorithms on BAM files. *Source Code for Biology and Medicine* **9** (2014).

38 Jones, D. T. *et al.* Dissecting the genomic complexity underlying medulloblastoma. *Nature* **488**, 100-105, doi:10.1038/nature11284 (2012).

39 Rimmer, A. *et al.* Integrating mapping-, assembly- and haplotype-based approaches for calling variants in clinical sequencing applications. *Nature genetics* **46**, 912-918, doi:10.1038/ng.3036 (2014).

40 Wang, K., Li, M. & Hakonarson, H. ANNOVAR: functional annotation of genetic variants from high-throughput sequencing data. *Nucleic acids research* **38**, e164, doi:10.1093/nar/gkq603 (2010).
41 Dobin, A. *et al.* STAR: ultrafast universal RNA-seq aligner. *Bioinformatics* **29**, 15-21, doi:10.1093/bioinformatics/bts635 (2013).
42 Quinlan, A. R. & Hall, I. M. BEDTools: a flexible suite of utilities for comparing genomic features. *Bioinformatics* **26**, 841-842, doi:10.1093/bioinformatics/btq033 (2010).
43 Korbel, J. O. & Campbell, P. J. Criteria for inference of chromothripsis in cancer genomes. *Cell* **152**, 1226-1236, doi:10.1016/j.cell.2013.02.023 (2013).
44 Verhaak, R. G. *et al.* Integrated genomic analysis identifies clinically relevant subtypes of glioblastoma characterized by abnormalities in PDGFRA, IDH1, EGFR, and NF1. *Cancer cell* **17**, 98-110, doi:10.1016/j.ccr.2009.12.020 (2010).
45 Roring, M. *et al.* Distinct requirement for an intact dimer interface in wild-type, V600E and kinase-dead B-Raf signalling. *EMBO J* **31**, 2629-2647, doi:10.1038/emboj.2012.100 (2012).
46 Eisenhardt, A. E. *et al.* Functional characterization of a BRAF insertion mutant associated with pilocytic astrocytoma. *International journal of cancer. Journal international du cancer* **129**, 2297-2303, doi:10.1002/ijc.25893 (2011).

Supplementary Data

Supplementary Figure 1-6 will be provided as a separate file.

Supplementary Table 1-5 will be provided as an Excel sheet.

Figure 1

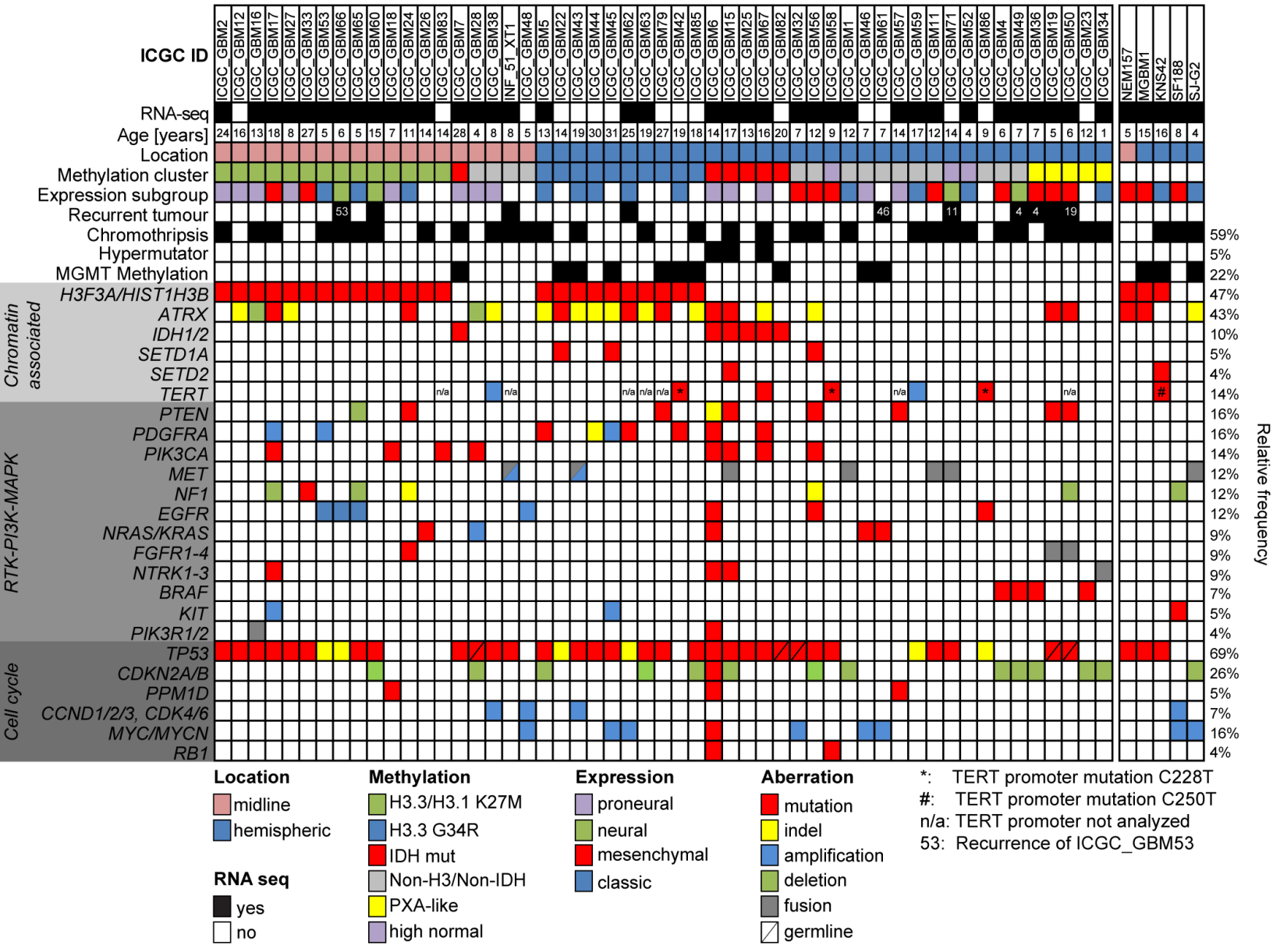
ICGC ID
ICGC_GBM2
ICGC_GBM12
ICGC_GBM16
ICGC_GBM17
ICGC_GBM27
ICGC_GBM33
ICGC_GBM53
ICGC_GBM66
ICGC_GBM65
ICGC_GBM60
ICGC_GBM18
ICGC_GBM24
ICGC_GBM26
ICGC_GBM83
ICGC_GBM7
ICGC_GBM28
ICGC_GBM38
INF_51_XT1
ICGC_GBM48
ICGC_GBM5
ICGC_GBM22
ICGC_GBM43
ICGC_GBM44
ICGC_GBM45
ICGC_GBM62
ICGC_GBM63
ICGC_GBM79
ICGC_GBM42
ICGC_GBM85
ICGC_GBM6
ICGC_GBM15
ICGC_GBM25
ICGC_GBM67
ICGC_GBM82
ICGC_GBM32
ICGC_GBM56
ICGC_GBM58
ICGC_GBM1
ICGC_GBM46
ICGC_GBM61
ICGC_GBM57
ICGC_GBM59
ICGC_GBM11
ICGC_GBM71
ICGC_GBM52
ICGC_GBM86
ICGC_GBM4
ICGC_GBM49
ICGC_GBM36
ICGC_GBM19
ICGC_GBM50
ICGC_GBM23
ICGC_GBM34
NEM157
MGBM1
KNS42
SF188
SJ-G2
RNA-seq
Age [years]
Location
Methylation cluster
Expression subgroup
Recurrent tumour
Chromothripsis
Hypermutator
MGMT Methylation
Chromatin associated
H3F3A/HIST1H3B
ATRX
IDH1/2
SETD1A
SETD2
TERT
RTK-PI3K-MAPK
PTEN
PDGFRA
PIK3CA
MET
NF1
EGFR
NRAS/KRAS
FGFR1-4
NTRK1-3
BRAF
KIT
PIK3R1/2
Cell cycle
TP53
CDKN2A/B
PPM1D
CCND1/2/3, CDK4/6
MYC/MYCN
RB1
59%
5%
22%
47%
43%
10%
5%
4%
14%
16%
16%
14%
12%
12%
12%
9%
9%
9%
7%
5%
4%
69%
26%
5%
7%
16%
4%
Relative frequency
Location
midline
hemispheric
RNA seq
yes
no
Methylation
H3.3/H3.1 K27M
H3.3 G34R
IDH mut
Non-H3/Non-IDH
PXA-like
high normal
Expression
proneural
neural
mesenchymal
classic
Aberration
mutation
indel
amplification
deletion
fusion
germline
*: TERT promoter mutation C228T
#: TERT promoter mutation C250T
n/a: TERT promoter not analyzed
53: Recurrence of ICGC_GBM53

Figure 2

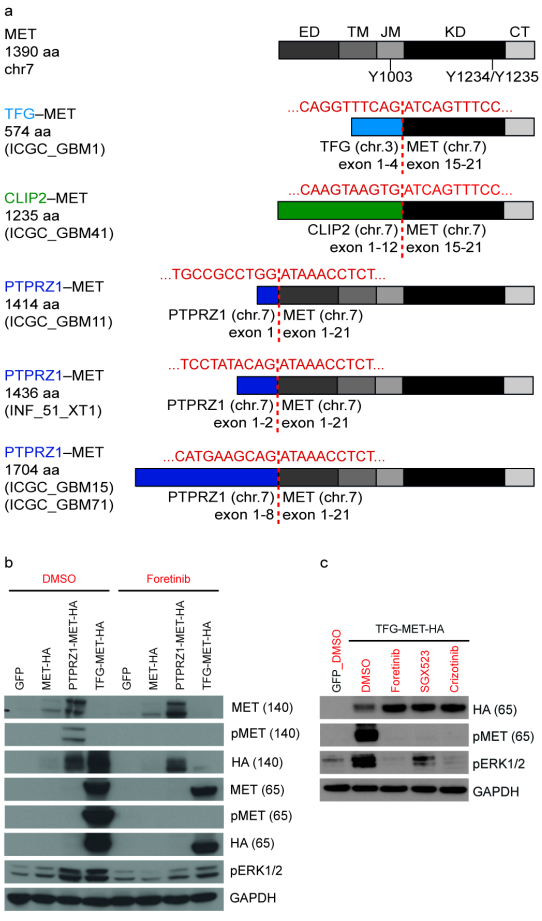
a
MET
1390 aa
chr7
ED
TM
JM
KD
CT
Y1003
Y1234/Y1235
TFG–MET
574 aa
(ICGC_GBM1)
...CAGGTTTCAG|ATCAGTTTCC...
TFG (chr.3)
MET (chr.7)
exon 1-4
exon 15-21
CLIP2–MET
1235 aa
(ICGC_GBM41)
...CAAGTAAGTG|ATCAGTTTCC...
CLIP2 (chr.7)
MET (chr.7)
exon 1-12
exon 15-21
PTPRZ1–MET
1414 aa
(ICGC_GBM11)
...TGCCGCCTGG|ATAAACCTCT...
PTPRZ1 (chr.7)
MET (chr.7)
exon 1
exon 1-21
PTPRZ1–MET
1436 aa
(INF_51_XT1)
...TCCTATACAG|ATAAACCTCT...
PTPRZ1 (chr.7)
MET (chr.7)
exon 1-2
exon 1-21
PTPRZ1–MET
1704 aa
(ICGC_GBM15)
(ICGC_GBM71)
...CATGAAGCAG|ATAAACCTCT...
PTPRZ1 (chr.7)
MET (chr.7)
exon 1-8
exon 1-21
b
DMSO
Foretinib
GFP
MET-HA
PTPRZ1-MET-HA
TFG-MET-HA
MET (140)
pMET (140)
HA (140)
MET (65)
pMET (65)
HA (65)
pERK1/2
GAPDH
c
TFG-MET-HA
GFP_DMSO
DMSO
Foretinib
SGX523
Crizotinib
HA (65)
pMET (65)
pERK1/2
GAPDH

Figure 3

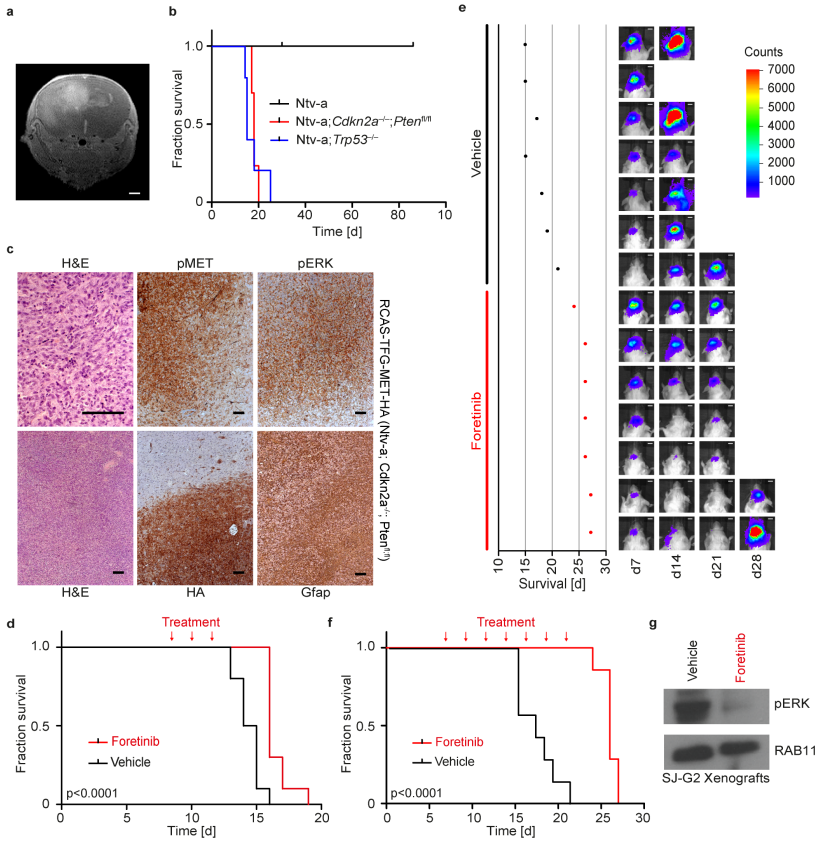
a
b
1.0
0.5
0
Fraction survival
0
20
40
60
80
10
Time [d]
Ntv-a
Ntv-a;Cdkn2a−/−;Ptenfl/fl
Ntv-a;Trp53−/−
c
H&E
pMET
pERK
H&E
HA
Gfap
RCAS-TFG-MET-HA (Ntv-a; Cdkn2a−/−; Ptenfl/fl)
e
Vehicle
Foretinib
10
15
20
25
30
Survival [d]
Counts
7000
6000
5000
4000
3000
2000
1000
d7
d14
d21
d28
d
Treatment
1.0
0.5
0
Fraction survival
Foretinib
Vehicle
p<0.0001
0
5
10
15
20
Time [d]
f
Treatment
1.0
0.5
0
Fraction survival
Foretinib
Vehicle
p<0.0001
0
5
10
15
20
25
30
Time [d]
g
Vehicle
Foretinib
pERK
RAB11
SJ-G2 Xenografts

Figure 4

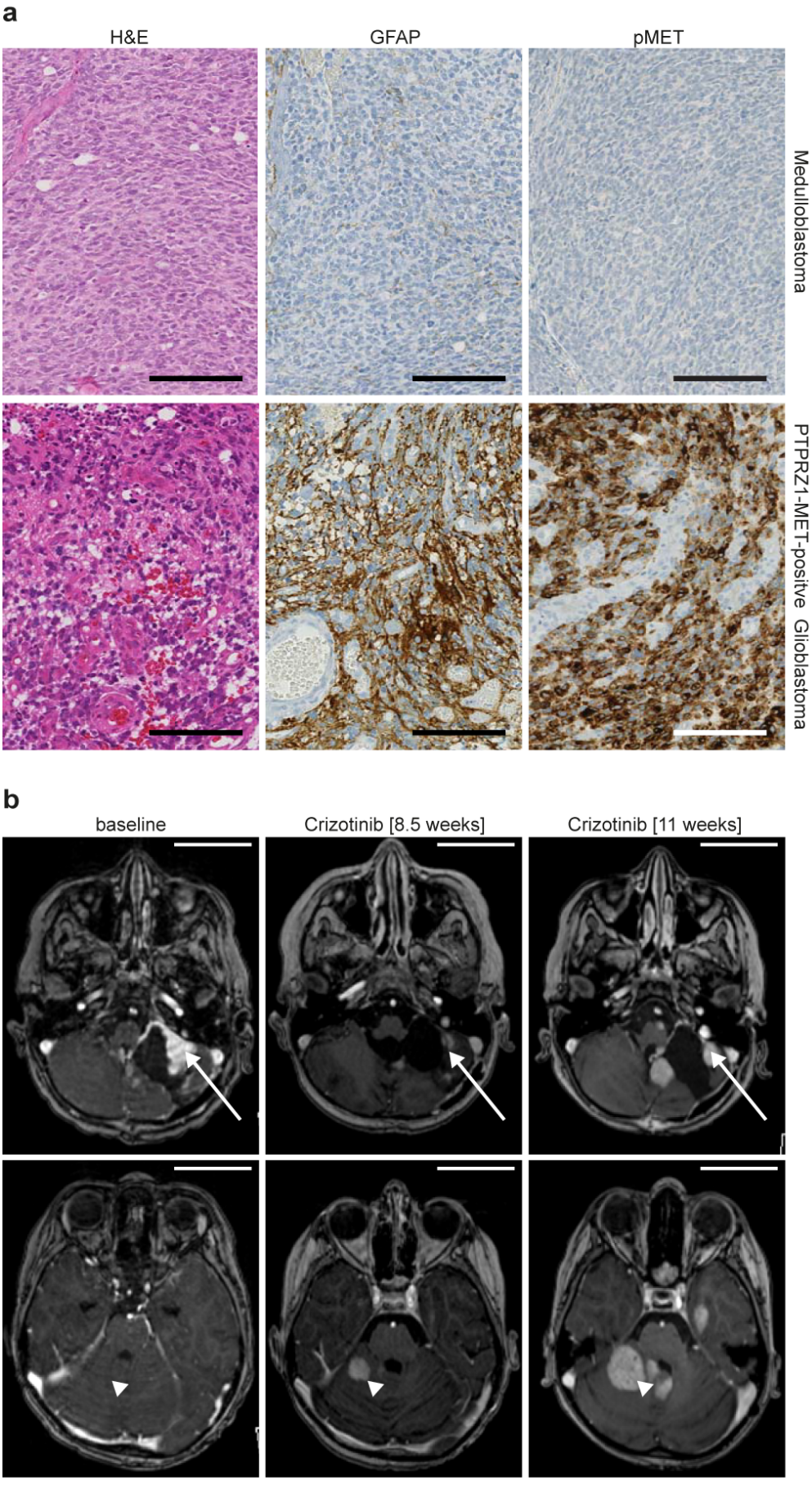
a
H&E
GFAP
pMET
Medulloblastoma
PTPRZ1-MET-positive Glioblastoma
b
baseline
Crizotinib [8.5 weeks]
Crizotinib [11 weeks]